

ZLI4792. Measured transmission difference maxima agree within experimental error, confirming that chiral GLAD films induce a type of chiral order in simple nematic LCs, similar to the chiral nematic phase seen in CLCs, and with the pitch matching the physical pitch of the GLAD helical columns.

Absolute transmission and normalized transmission difference through the film impregnated with the nematic E7 are shown in Fig. 3. Here the observed transmission difference is much stronger than that observed with the C3M and ZLI4792 impregnates. Again, the maxima occurs (within experimental error) at the wavelength predicted assuming chiral nematic order of the LC within the GLAD film. Figure 3b shows a calculated curve from equation (1) where the transmission difference peak magnitude and wavelength have been chosen to match the measured spectrum. In matching the measured curve, an average index of $n_{\text{avg}} = 1.43$ and an anisotropy $\delta = 0.024$ were used. The simple mixing rule described above predicts an average index of $n_{\text{avg}} = 1.47$, again within experimental error. The optical anisotropy is much less than that of E7 alone ($\delta \approx 0.14$), but as the hybrid is composed of 60% isotropic MgF_2 , and 40% LC, this is not unexpected. It is quite difficult to estimate the anisotropy for the composite material and this was not attempted.

Differential transmission of circularly polarized light through the hybrid thin-film/LC material shows that some chiral ordering of the LC is induced by the helical backbone of the porous film fabricated with GLAD. However, a true single-domain 'planar' chiral nematic texture, where all LC molecules lie parallel to the substrate with the helical axis perpendicular, is not the only possible molecular orientational texture. The observed differences in effect with varying material (E7 produced much stronger Bragg reflection than the other LCs), as well as the low anisotropy needed to match theory to observations in Fig. 3b, suggest that a more complicated alignment in fact occurs. One peculiarity of the LC E7 is that there is a cyano group at the end of the rod-like molecules. Dipole interactions of this group with polar surfaces (such as glass) make these molecules susceptible to alignment perpendicular to the surface (homeotropic alignment). It is therefore likely that at the surfaces of the MgF_2 helices, the E7 molecules will align homeotropically. But in the larger voids between the helical MgF_2 columns, the complex mix of alignments arising from homeotropic alignment onto helical columns must resolve to reduce elastic energies. One possible texture is a tilted orientation that follows the rotation of the nearby helices. The 'bulk' void regions would have a chiral texture that imitates the nearby helices, but with a tilt to reduce elastic energy and eliminate domain boundaries. Another possibility would be a tube-like structure with homeotropic alignment (perpendicular to the substrate) within the 'bulk' void regions. This texture is more like that seen in the absence of a helical backbone, where all molecules are aligned homeotropically (perpendicular to the substrate). The MgF_2 columns would then introduce small but periodic variations in the local orientation of the LC near the columns. These two possible textures probably describe the limits of a continuum of alignments; the alignment that occurred would depend on the inorganic film material and surface treatments, LC chemistry, temperature and applied fields. Both possibilities would help to explain the low observed anisotropy of the E7 mixture, as the full anisotropy of the tilted LC is not seen for light propagating along the helical axis.

As an example, and as a comparison to conventional LC techniques, one of us (D.J.B.) has shown that the small bandwidth of transmission/reflection (usually <100 nm) of a CLC layer can be increased by producing a structure with a graded pitch. This was accomplished by crosslinking reactive CLCs by photopolymerization of a diffusion-controlled concentration gradient of CLC²³. This produced a solidified structure, however, and does not allow for switching. The GLAD technique allows LC alignment structures, such as graded pitches, to be engineered for a desired optical response, and will still allow switching of the LC. GLAD films

composed of multiple layers with different pitches, handedness and structure have been fabricated, and will be investigated in future work. □

Received 26 February; accepted 5 May 1999.

1. Crawford, G. P. & Zumer, S. (eds) *Liquid Crystals in Complex Geometries* (Taylor and Francis, London, 1996).
2. Robbie, K. & Brett, M. J. Sculptured thin films and glancing angle deposition: growth mechanics and applications. *J. Vac. Sci. Technol. A* **15**, 1460–1465 (1997).
3. Robbie, K., Sit, J. C. & Brett, M. J. Advanced techniques for glancing angle deposition. *J. Vac. Sci. Technol. B* **16**, 1115–1122 (1998).
4. Belyakov, V. A. & Dmitrienko, V. E. Optics of chiral liquid crystals. *Sov. Sci. Rev. A* **13**, (1989).
5. Young, N. O. & Kowal, J. Optically active fluorite films. *Nature* **183**, 104–105 (1959).
6. Azzam, R. M. A. Chiral thin solid films: method of deposition and applications *Appl. Phys. Lett.* **61**, 3118–3120 (1992).
7. Hodgkinson, I. J. & Wu, Q. H. *Birefringent Thin Films and Polarizing Elements* (World Scientific, Singapore, 1997).
8. van Kranenburg, H. & Lodder, J. C. Tailoring growth and local composition by oblique-incidence deposition: a review and new experimental data. *Mater. Sci. Eng. R* **11**, 295–354 (1994).
9. Robbie, K., Friedrich, L. J., Dew, S. K., Smy, T. & Brett, M. J. Fabrication of thin films with highly porous microstructures. *J. Vac. Sci. Technol. A* **13**, 1032–1035 (1995).
10. Lakhtakia, A. & Weiglhofer, W. S. On light propagation in helicoidal bianisotropic mediums. *Proc. R. Soc. Lond. A* **448**, 419–437 (1995).
11. Robbie, K., Brett, M. J. & Lakhtakia, A. First thin film realization of a helicoidal bianisotropic medium. *J. Vac. Sci. Technol. A* **13**, 2991–2993 (1995).
12. Robbie, K., Brett, M. J. & Lakhtakia, A. Chiral sculptured thin films. *Nature* **384**, 616 (1996).
13. Rovira, P. I. et al. Rotating-compensator multichannel transmission ellipsometry of a thin-film helicoidal bianisotropic medium. *Thin Solid Films* **313–314**, 373–378 (1998).
14. Barron, L. D. *Molecular Light Scattering and Optical Activity* (Cambridge Univ. Press, 1982).
15. Chandrasekhar, S. *Liquid Crystals* (Cambridge Univ. Press, 1977).
16. Robbie, K., Hnatiw, A. J. P., Brett, M. J., MacDonald, R. I. & McMullin, J. N. Inhomogeneous thin film optical filters fabricated using glancing angle deposition. *Electron. Lett.* **33**, 1213–1214 (1997).
17. Sit, J. C., Vick, D., Robbie, K. & Brett, M. J. Thin film microstructural control using glancing angle deposition by sputtering. *J. Mater. Res.* **14**, 1197–1199 (1999).
18. Xu, F., Kitzerow, H.-S. & Crooker, P. P. Electric-field effects on nematic droplets with negative dielectric anisotropy. *Phys. Rev. E* **46**, 6535–6540 (1992).
19. Ondris-Crawford, R. J. et al. Surface molecular anchoring in microconfined liquid crystals near the nematic-smectic-A transition. *Phys. Rev. E* **48**, 1998–2005 (1993).
20. Berreman, D. W. Optics in stratified and anisotropic media: 4×4 -matrix formulation. *J. Opt. Soc. Am.* **62**, 502–510 (1972).
21. St John, W. D., Fritze, W. J., Lu, Z. J. & Yang, D.-K. Bragg reflection from cholesteric liquid crystals. *Phys. Rev. E* **51**, 1191–1198 (1995).
22. Xu, M., Xu, F. & Yang, D.-K. Effects of cell structure on the reflection of cholesteric liquid crystal displays. *J. Appl. Phys.* **83**, 1938–1944 (1998).
23. Broer, D. J., Lub, J. & Mol, G. N. Wide-band reflective polarizers from cholesteric polymer networks with a pitch gradient. *Nature* **378**, 467–469 (1995).

Acknowledgements. This work was supported in part by the Natural Sciences and Engineering Council of Canada and the Alberta Microelectronic Centre.

Correspondence and requests for materials should be addressed to K.R. at Queen's University (e-mail: robbie@physics.queensu.ca).

A reversibly antigen-responsive hydrogel

Takashi Miyata, Noriko Asami & Tadashi Uragami

Chemical Branch, Faculty of Engineering and High Technology Research Center, Kansai University, Suita, Osaka, 564-8680, Japan

Stimuli-responsive hydrogels that undergo abrupt changes in volume in response to external stimuli such as pH, temperature and solvent composition have potential applications in biomedicine and the creation of 'intelligent' materials systems, for example as media for drug delivery, separation processes and protein immobilization. Hydrogels have been reported that respond to pH^{1–3}, temperature^{4–13}, electric fields^{14–16} and saccharides^{17–22}. For some biomedical applications it would be very useful to have a material whose swelling response was dictated by a specific protein. Here we report such a material, which swells reversibly in a buffer solution in response to a specific antigen. The hydrogel was prepared by grafting the antigen and corresponding antibody to the polymer network, so that binding between the two introduces crosslinks in the network. Competitive binding of the free antigen triggers a change in gel volume owing to breaking of these non-covalent crosslinks. In addition, we show that the hydrogel displays shape-memory behaviour, and that stepwise changes in antigen concentration can induce pulsatile permeation of a

protein through the network.

Our strategy is to use the reversible binding between an antigen and an antibody as the crosslinking mechanism in a semi-interpenetrating network (semi-IPN) hydrogel (Fig. 1a). The hydrogel can swell in the presence of a free antigen because the intra-chain antigen-antibody binding can be dissociated by exchange of the grafted antigen for free antigen. In the absence of a free antigen, the

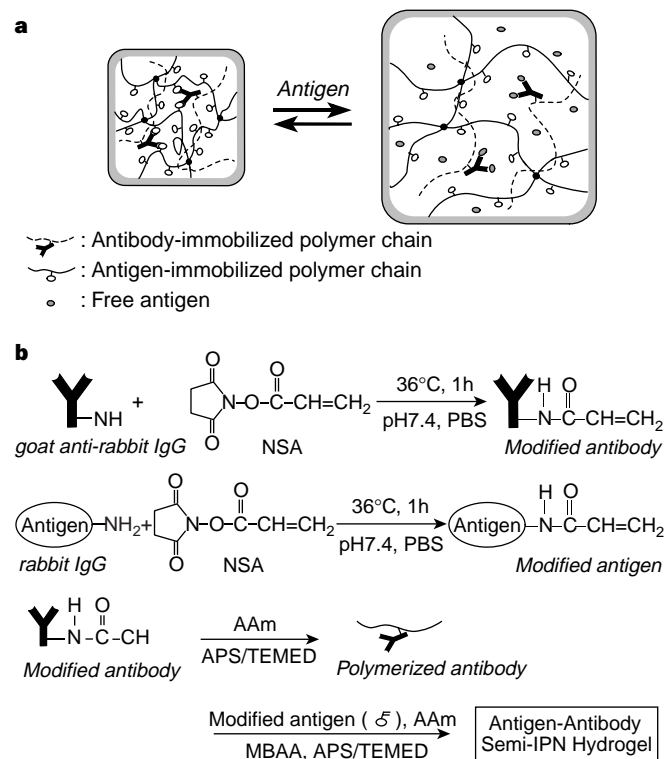


Figure 1 Strategy for the preparation of an antigen-responsive hydrogel. **a**, Diagram of a suggested mechanism for the swelling of an antigen-antibody semi-IPN hydrogel in response to a free antigen. **b**, Synthesis of the antigen-antibody semi-IPN hydrogel. The GAR IgG was chemically modified by coupling it with *N*-succinimidylacrylate (NSA) in phosphate buffer solution, using the method reported by Hoffman *et al.*²³. NSA (0.4 mg) was added to a phosphate buffer solution (0.02 M, pH 7.4) containing the GAR IgG (100 mg) (NSA/GAR IgG molar ratio is 6:1), and the reaction was then incubated at 36 °C for one hour to introduce the vinyl groups into the GAR IgG. The resultant vinyl(GAR IgG) was purified by gel filtration, and a phosphate buffer solution containing the vinyl(GAR IgG) was obtained at a concentration of 1.91 mg ml⁻¹. After acrylamide (AAm) (30 mg) was added to 570 mg of the vinyl(GAR IgG) solution, together with 0.01 ml of 0.1 M aqueous ammonium persulphate (APS) and 0.01 ml of 0.8 M aqueous *N,N,N',N'*-tetramethylethylenediamine (TEMED) as redox initiators, the copolymerization was performed at 25 °C for 3 h to synthesize the polymerized GAR IgG. As the relative molecular mass of the resultant polymerized GAR IgG was ~220,000, the average number of IgG incorporated into a polymerized GAR IgG was ~1. Furthermore, vinyl(rabbit IgG) was also synthesized by modifying rabbit IgG with NSA in the same manner as the vinyl(GAR IgG). The resultant vinyl(rabbit IgG) (2.46 mg), AAm (82 mg) and *N,N'*-methylenebisacrylamide (MBAA) (0.1 wt% relative to AAm) as a crosslinker were dissolved in 600 mg of phosphate buffer solution containing the polymerized GAR IgG to form the antigen-antibody binding. As soon as 0.01 ml of 0.1 M aqueous APS and 0.01 ml of 0.8 M aqueous TEMED were added into the mixture as redox initiators, it was injected into a glass capillary tube with an inner diameter of 3 mm (or into a mould membrane preparation), and the polymerization was performed at 25 °C for 3 h. After the polymerization, the resultant antigen-antibody semi-IPN hydrogels were immersed in phosphate buffer to remove any residual chemicals and unreacted monomers. Polyacrylamide (PAAm) semi-IPN hydrogels were also prepared as a reference material by the redox copolymerization of AAm and MBAA in the presence of linear PAAm in the same manner.

hydrogel shrinks. We used rabbit immunoglobulin G (rabbit IgG) and goat anti-rabbit IgG (GAR IgG) as the antigen and antibody, respectively. The GAR IgG was purified with an affinity column in which rabbit IgG was immobilized; the binding of those IgGs formed the stimuli-responsive crosslinking point in the hydrogel. The typical method to prepare antigen-antibody semi-IPN hydrogel is shown in Fig. 1b. The rabbit IgG and GAR IgG were chemically modified by coupling them with *N*-succinimidylacrylate (NSA in Fig. 1b) in phosphate buffer solution, using the method reported by Hoffman *et al.*²³. The copolymerization of the resultant vinyl(GAR IgG) with acrylamide (AAm) was performed with redox initiators to synthesize the polymerized GAR IgG. An antigen-antibody semi-IPN hydrogel was prepared by the copolymerization of the vinyl(rabbit IgG), acrylamide and *N,N'*-methylenebisacrylamide (MBAA) as a cross-linker in the presence of the polymerized GAR IgG in a glass capillary tube.

The antigen-responsive swelling of the antigen-antibody and polyacrylamide semi-IPN hydrogels was examined after their swelling attained equilibrium in 0.2 M phosphate buffer solution (pH 7.4); the water content of the equilibrated hydrogels was 97 wt%. The swelling ratio of the antigen-antibody semi-IPN hydrogel increased abruptly following the addition of free rabbit IgG. Furthermore, the swelling ratio of the polyacrylamide semi-IPN hydrogel was independent of the antigen concentration in the buffer solution, but the swelling ratio of the antigen-antibody semi-IPN hydrogel was strongly dependent upon it (Fig. 2). This indicates that the latter hydrogel is rabbit-IgG-responsive, and has an antigen-sensing function.

To determine the mechanism responsible for the rabbit-IgG-responsive swelling, complex formation between the antigen and antibody in the hydrogel was investigated using the BIAcore system^{24,25} (Pharmacia Biotec, Inc.). GAR IgG was immobilized on a sensor tip surface in the BIAcore system; the surface plasmon resonance induced at the interface between the surface and the solution containing modified rabbit IgG was then examined to determine the kinetic parameter for the complex formation. As a result, the binding constants of the GAR IgG to the native and polymerized rabbit IgGs were $8.90 \times 10^8 \text{ M}^{-1}$ and $2.61 \times 10^8 \text{ M}^{-1}$, respectively. This suggests that the binding of the GAR IgG with rabbit IgG polymerized in the antigen-antibody hydrogel was much weaker than to native rabbit IgG, due to the denaturation of the modified rabbit IgG. Therefore, adding free native rabbit IgG can induce the dissociation of the complex between GAR IgG and rabbit IgG grafted to the semi-IPN hydrogel.

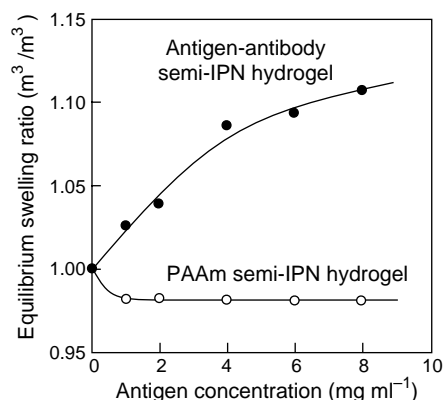


Figure 2 Effects of the free antigen concentration on the hydrogel swelling ratio. Shown is the equilibrium swelling ratio of the PAAm semi-IPN hydrogel (open circles) and the antigen-antibody semi-IPN hydrogel (filled circles) in phosphate buffer solution at 25 °C as a function of antigen concentration in the buffer solution. The swelling ratio of the hydrogels was determined by the ratio of their changing diameters, which were measured in the solution using an optical microscope.

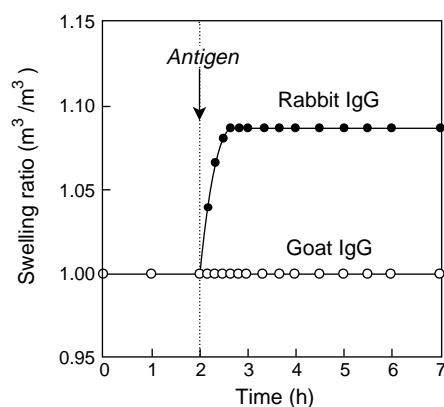


Figure 3 Antigen recognition by the antigen-antibody semi-IPN hydrogel. The swelling ratio of the antigen-antibody semi-IPN hydrogel is shown, before and after the addition of goat IgG (open circles) and rabbit IgG (filled circles). Measurements were made after the swelling had attained equilibrium in phosphate buffer solution at 25 °C. The concentration of the antigen in the phosphate buffer solution was 4 mg ml⁻¹.

The crosslinking density of a hydrogel can be determined by measuring its compressive modulus^{10,18,26}. We performed compressive modulus measurements to examine the changes in the crosslinking density of the hydrogel following the addition of free antigen (see Supplementary Information). The crosslinking density decreased gradually in proportion to the increasing free rabbit IgG concentration in the phosphate buffer solution, indicating that the antigen-responsive swelling changes are due to decreasing crosslinking density, which is consistent with the mechanism depicted in Fig. 1a. We note that the denaturation of the rabbit IgG in preparing the antigen-responsive hydrogel was an important factor in the exchange between native and polymerized rabbit IgGs.

The swelling ratio of the hydrogel did not change following the addition of goat IgG, whereas addition of rabbit IgG led to a drastic increase (Fig. 3). These results mean that the hydrogel can recognize a specific antigen and change its structure chemomechanically. As the GAR IgG in the hydrogel forms a complex with rabbit IgG only due to the excellent antigen-recognition of this antibody, the addition of goat IgG results in no dissociation of the complex between the rabbit IgG and the GAR IgG grafted to the hydrogel.

Most potential applications of the antigen-antibody semi-IPN hydrogel require that the swelling be reversible. We investigated the reversibility in response to stepwise changes in the antigen concentration, as well as the consequent permeation of a model protein drug (haemoglobin) through a membrane fabricated from the hydrogel. Figure 4 shows the swelling ratio of the polyacrylamide and antigen-antibody semi-IPN hydrogels, and permeation profiles of a model protein drug through their membranes, as a function of time; during this time, they were alternately immersed in phosphate buffer with and without 4 mg ml⁻¹ of rabbit IgG. There was no change in the swelling ratio of the polyacrylamide semi-IPN hydrogel following its alternate immersion in phosphate buffer with and without rabbit IgG. However, the antigen-antibody semi-IPN hydrogel swelled immediately in the presence of rabbit IgG, and shrank gradually in its absence. In contrast, another antigen-antibody hydrogel without a semi-IPN structure also swelled following the addition of free rabbit IgG, but did not shrink following immersion in phosphate buffer without rabbit IgG (data not shown). This suggests that the semi-IPN structure is important in the reversibility of the antigen-responsive swelling changes. In the semi-IPN hydrogel the grafted GAR IgG is trapped in a network containing grafted rabbit IgG, and so the hydrogel can shrink reversibly because the crosslinks between grafted GAR IgG and grafted rabbit IgG reform in phosphate buffer (Fig. 1a). Furthermore, because the hydrogel was prepared by copolymerizing with

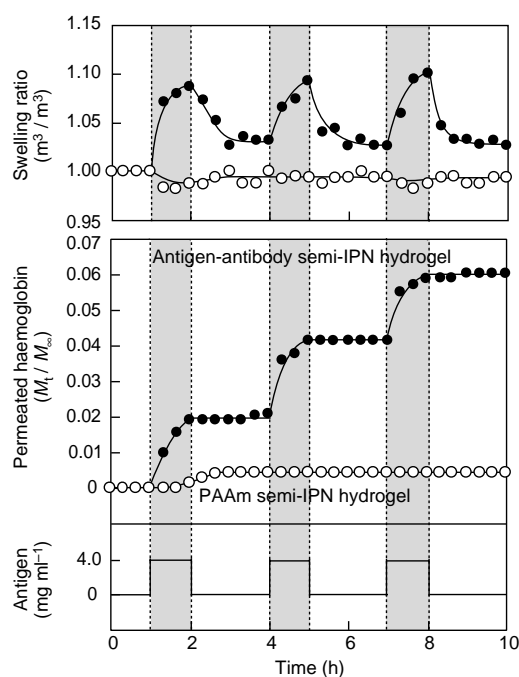


Figure 4 Reversible swelling changes and antigen-responsive permeation profiles. Shown are swelling ratio changes of the PAAm semi-IPN hydrogel (open circles) and the antigen-antibody semi-IPN hydrogel (filled circles), and a permeation profile of a model drug through their membranes, in response to stepwise changes in the antigen concentration between 0 and 4 mg ml⁻¹ at 25 °C. Permeation experiments were performed at 25 °C with magnetic stirring, using a glass cell of two parts separated by a hydrogel membrane. One chamber of the cell was filled with phosphate buffer solution containing haemoglobin (1 mg ml⁻¹) as a model protein drug, and other chamber was filled with a phosphate buffer solution in which the antigen concentration was changed stepwise between 0 and 4 mg ml⁻¹. M_t indicates the amount of the model drug permeated through the hydrogel membrane at a given time; M_∞ indicates the total amount of the model drug in the chamber of the cell.

vinyl(rabbit IgG), which forms a complex with the polymerized GAR IgG, the resultant semi-IPN hydrogel can ‘memorize’ the shape of its initial semi-IPN structure. Thus, hydrogel shrinks in the absence of rabbit IgG on the basis of a ‘shape-memory-like’ effect. In addition, it is apparent from Fig. 4 that the model drug permeates through the membrane in the presence of rabbit IgG but is stopped in its absence, suggesting that this approach might permit drug delivery in response to a specific antigen. □

Received 19 October 1998; accepted 19 April 1999.

1. Tanaka, T. Collapse of gels and the critical endpoint. *Phys. Rev. Lett.* **40**, 820–823 (1978).
2. Tanaka, T. *et al.* Phase transitions in ionic gels. *Phys. Rev. Lett.* **45**, 1636–1639 (1980).
3. Siegel, R. A. & Firestone, B. A. pH-dependent equilibrium swelling properties of hydrophobic polyelectrolyte copolymer gels. *Macromolecules* **21**, 3254–3259 (1988).
4. Hirokawa, Y. & Tanaka, T. Volume phase transition in a nonionic gel. *J. Chem. Phys.* **81**, 6379–6380 (1984).
5. Hoffman, A. S. Applications of thermally reversible polymers and hydrogels in therapeutics and diagnostics. *J. Controlled Release* **6**, 297–305 (1987).
6. Bae, Y. H., Okano, T., Hsu, R. & Kim, S. W. Thermo-sensitive polymers as on-off switches for drug release. *Makromol. Chem. Rapid Commun.* **8**, 481–485 (1987).
7. Bae, Y. H., Okano, T. & Kim, S. W. A new thermo-sensitive hydrogel: interpenetrating polymer networks from N-acryloylpyrrolidine and poly(oxethylene). *Makromol. Chem. Rapid Commun.* **9**, 185–189 (1988).
8. Chen, G. & Hoffman, A. S. Graft copolymers that exhibit temperature-induced phase transitions over a wide range of pH. *Nature* **373**, 49–52 (1995).
9. Yoshida, R. *et al.* Comb-type grafted hydrogels with rapid de-swelling response to temperature changes. *Nature* **374**, 240–242 (1995).
10. Miyata, T., Nakamae, K., Hoffman, A. S. & Kanzaki, Y. Stimuli-sensitivities of hydrogels containing phosphate groups. *Macromol. Chem. Phys.* **195**, 1111–1120 (1994).
11. Aoki, T. *et al.* Temperature-responsive interpenetrating polymer networks constructed with poly(acrylic acid) and poly(N,N-dimethylacrylamide). *Macromolecules* **27**, 947–952 (1994).
12. Stayton, P. S. *et al.* Control of protein-ligand recognition using a stimuli-responsive polymer. *Nature* **378**, 472–474 (1995).
13. Feil, H., Bae, Y. H., Feijen, J. & Kim, S. W. Molecular separation by thermosensitive hydrogel membranes. *J. Membrane Sci.* **64**, 283–294 (1991).

14. Tanaka, T., Nishio, I., Sun, S.-T. & Ueno-Nishio, S. Collapse of gels in an electric field. *Science* **218**, 467–469 (1982).
15. Kwon, I. C., Bae, Y. H. & Kim, S. W. Electrically erodible polymer gel for controlled release of drugs. *Nature* **354**, 291–293 (1991).
16. Osada, Y., Okuzaki, H. & Hori, H. A polymer gel with electrically driven motility. *Nature* **355**, 242–244 (1992).
17. Kokufuta, E., Zhang, Y.-Q. & Tanaka, T. Saccharide-sensitive phase transition of a lectin-loaded gel. *Nature* **351**, 302–304 (1991).
18. Miyata, T., Jikihara, A., Nakamae, K. & Hoffman, A. S. Preparation of poly(glucosyloxyethyl methacrylate)-concanavalin A complex hydrogel and its glucose-sensitivity. *Macromol. Chem. Phys.* **197**, 1135–1146 (1996).
19. Lee, S. J. & Park, K. Synthesis and characterization of sol-gel phase-reversible hydrogels sensitive to glucose. *J. Mol. Recogn.* **9**, 549–557 (1996).
20. Obidat, A. A. & Park, K. Characterization of glucose dependent gel-sol phase transition of polymeric glucose-concanavalin A hydrogel system. *Pharm. Res.* **13**, 989–995 (1996).
21. Obidat, A. A. & Park, K. Characterization of protein release through glucose-sensitive hydrogel membranes. *Biomaterials* **18**, 801–806 (1997).
22. Kataoka, K. *et al.* Totally synthetic polymer gels responding to external glucose concentration: their preparation and application to on-off regulation of insulin release. *J. Am. Chem. Soc.* **120**, 12694–12695 (1998).
23. Shoemaker, S. G., Hoffman, A. S. & Priest, J. H. Synthesis and properties of vinyl monomer/enzyme conjugates. *Appl. Biochem. Biotech.* **15**, 11–24 (1987).
24. Natsume, T. *et al.* Interactions between collagen-binding stress protein HSP47 and collagen. *J. Biol. Chem.* **269**, 31224–31228 (1994).
25. Murai, N., Taguchi, H. & Yoshida, M. Kinetic analysis of interactions between GroEL and reduced α -lactalbumin. *J. Biol. Chem.* **270**, 19957–19963 (1995).
26. Flory, P. J. *Principles of Polymer Chemistry* (Cornell Univ. Press, New York, 1953).

Supplementary information is available on Nature's World-Wide Web site (<http://www.nature.com>) or as paper copy from the London editorial office of Nature.

Correspondence and requests for materials should be addressed to T.M. (e-mail: tmiyata@ipcku.kansai-u.ac.jp).

The use of path integration to guide route learning in ants

B. Schatz*, S. Chameron†, G. Beugnon† & T. S. Collett*

* *Sussex Centre of Neuroscience, School of Biological Sciences, University of Sussex, Brighton BN1 9QG, UK*

† *Laboratoire d'Ethologie et de Psychologie Animale, CNRS-UMR 5550, Université Paul-Sabatier, Toulouse cedex 04, France*

Cataglyphid ants travelling between their nest and feeding site follow familiar routes along which they are guided by views of the surrounding landscape^{1–5}. On bare terrain, with no landmarks available, ants can still navigate using path integration⁶. They continually monitor their net distance and direction from the nest, so that they can return home from any point using their computed 'home vector'⁷. Here we ask whether path integration also provides signals to reinforce the learning of visual landmarks. A fall in the value of the home vector indicates when a homing ant moves in roughly the correct direction, and that it is appropriate to store those views that can guide subsequent trips to the nest⁸. We tested this hypothesis by training the ant *Cataglyphis cursor* to negotiate a variety of mazes that led from a feeding site back to the nest. Efficient passage of each maze required an ant to discriminate between different pairs of shapes⁹. We show that if the value of the home vector drops while the ant approaches and passes a shape, the shape's appearance is learnt, but if the vector grows, or is absent, no visual learning occurs. Path integration may both help ants navigate through an unfamiliar landscape, and assist them to become familiar with it.

Cataglyphis cursor is a mediterranean ant with a mean foraging range of 6 m (ref. 10) and it readily forages in the laboratory. Our first maze (Fig. 1a) was designed so that the home vector decreased as the ant travelled towards the nest from the feeder. Foragers from the nest reached a sucrose feeder through an unobstructed tunnel (122 cm). Individually marked foragers were taken from the feeder to a waiting box and then transferred singly to the start of the maze. The maze was directly above the tunnel and aligned with it. It had four compartments connected by passages. Each compartment had one entrance and two exits, of which one was blocked and the other led to the next compartment (Fig. 1a). Open and closed exits were

labelled by black shapes on a white background (Fig. 1a, inset). To prevent ants from negotiating the maze by following a fixed path, we changed the side of the open exit and its associated shape after each trial. Ants learn which visual shape signals the open exit in each compartment and their sequence along the maze⁹.

Four other combinations of maze and tunnel were devised in which the home vector increased, or was absent, over all or part of the ant's homeward passage through the maze. Instead of a linear tunnel and maze, the tunnel and/or the maze were bent into a U shape, so introducing a large discrepancy between the ant's direction and that of its home vector (Fig. 1b–e). Our aim was to test whether visual learning is impaired under these conditions.

The combined acquisition curves of a group of ants trained to reach food through the linear tunnel and to home along the linear maze are plotted separately for each compartment (Fig. 2a). Each plot cumulates, over successive trials, the mean number of errors made by each ant on its first choice of exit on each trial. With no learning, the curves should stick to the line indicating chance performance. In fact, the curves deviate significantly ($P < 0.01$) downwards from that line after 13, 11, 5 and 1 trials in compartments 1 to 4, respectively. During training, there was attrition in the number of ants, as shown by the numbers given at the top of each column. Of the 16 ants remaining at the end of the 100-trial observation period, 13 had learnt compartments 1 and 2, 16 had learnt compartment 3, and 15 had learnt compartment 4. We show in the Methods that the 1-trial score in compartment 4 can be explained by the ants' sensitivity to the alternating pattern used in training. Thus, the gradient in error scores over the four compartments may, to some extent, be a consequence of the ants' intrinsic motor strategies.

Visual learning was absent when the directions of the home vector and the maze differed. We trained ants to reach the feeder through a U-shaped tunnel, so that the presumed home vector was very short and, if directed at all, was perpendicular to the maze. The return to the nest was either through a U-shaped (Fig. 1b) or through a linear

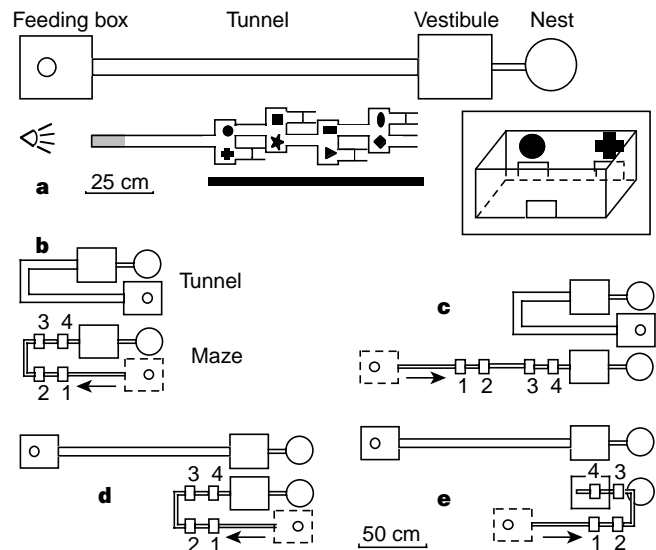


Figure 1 Diagrams of mazes used to test visual learning. In all conditions, the maze is placed directly over the tunnel. **a**, Ants approach the feeder along a linear tunnel and return home singly through a linear maze. The open exit from compartment 1 of the maze is labelled by a black circle, and the open exits from the other three compartments by a star, a rectangle and a diamond, respectively. Directional cues come from a floodlight at one end of the room and a large piece of black card fixed to one wall. Inset, three-dimensional sketch of one compartment to show ant's view of the shapes and exits. **b**, Tunnel and maze with same compartments and visual shapes as in **a** are both bent into a U shape. **c**, U-shaped tunnel and linear maze. **d, e**, Linear tunnel followed by a U-shaped maze. Upper calibration refers to **a**, lower calibration refers to **b–e**.